# Analysis and Design of a Non-Isolated Bidirectional DC-DC Converter with High Voltage Ratio for Battery Storage System

Dharavath Anusha
*Electrical Engineering Department*
*National Institute of Technology Warangal*
Warangal, India
danusha94@gmail.com

Srinivasan Pradabane
*Electrical Engineering Department*
*National Institute of Technology Warangal*
Warangal, India
spradabane@nitw.ac.in

2024 IEEE International Conference on Power Electronics, Drives and Energy Systems (PEDES) | 979-8-3503-7247-2/24/$31.00 ©2024 IEEE | DOI: 10.1109/PEDES61459.2024.10961159

***Abstract*—The energy storage system strengthens the grid resiliency and reliability and also has the ability to reduce greenhouse gas emissions. But the most energy storage sources such as batteries and ultra-capacitors, have low terminal voltage. To integrate these energy sources into hybrid system necessitate high voltage conversion ratio power electronic topologies to meet the load requirement of the system. Practically, the traditional step-up or step-down DC-DC converters are not feasible to meet a wide range of conversions. A hybrid structure of a bi-directional high-gain DC-DC converter (HGBDC) has been developed by integrating capacitors and inductors. This converter offers enhanced conversion ratio at lower duty ratios and enables bi-directional energy transfer with a simplified component layout while utilizing fewer semiconductors and passive components. The operational principles, steady-state analysis, and performance of this topology have been thoroughly explained. Additionally, a comprehensive comparative study has been conducted with the recent literature to show superiority of proposed converter. To validate the performance and feasibility of the proposed bidirectional converter MATLAB/Simulink simulation results for output power of 500 W are presented.**

***Keywords— step-up, step-down, battery storage, dc-link, non-isolated, DC-DC converter***

## I. INTRODUCTION

Global policies aimed at decarbonizing [1] energy are driving the adoption of variable renewable energy sources (RES) such as solar photo-voltaic cells (PVs), wind, fuel cells, and hydro power [2-3] in the widespread electrification of transportation. However, the intermittent and variable nature of these RES can impact their output reliability, often resulting in the generation of minimal and less dependable voltage ranges. To enhance RES reliability, energy storage devices (ESDs) such as batteries or super-capacitors are utilized. Power electronic conversion technologies act as intermediaries between low-voltage ESDs and the grids to facilitate smooth energy transfer and management within electrical systems [4]. Within this framework, there's a growing interest in leveraging the substantial energy storage capacity of electric vehicles (EVs) to support the integration of renewables, a concept known as vehicle-to-grid (V2G) and grid-to-vehicles (G2V). The idea entails charging EV batteries during off-peak periods of demand or when renewable generation is high, with the stored energy subsequently available to be fed back into the grid as reserve power. In order to fulfil mentioned requirements, a high-gain bidirectional DC-DC converter is required to employ in hybrid energy systems. These converter play a crucial role in transferring the power bi-directionally from the battery to grid.

Reliable and efficient high gain step-up and step-down DC-DC converters are used in multiple emerging applications such as battery storage, fuel cells, PV cells, LED lighting and X-ray power [5]. In order to fulfil mentioned requirements, a high-gain bidirectional DC-DC converter is required to employ in hybrid energy systems. These converter play a crucial role in transferring the power bi-directionally from the battery to grid and grid to battery. Therefore, developing a wide range of voltage gain bi-directional converters with fewer components is still a challenging task. Bi-directional converters face significant common limitations; low voltage gain, higher components counts, bulky, and low efficiency. Numerous bi-directional converters [6-15] documented in prior literature for various applications possess both pros and cons. Certainly, the conventional buck-boost converter [16] is suitable for achieving step-up/down voltage gain due to its simple structure and ease of control. However, in the conventional buck-boost converter, the power switch and output diode must withstand significant high voltage stresses and the input current ripple. Converters [6-7] have the voltages gains of $2/(1-D_H)$ and $D_L/2$ in step-up and step-down operations respectively. Converter [6] have low voltage stress and reduced current ripple but it uses more number of components. Where converter [7] uses a minimal number of components, but it can only achieve a limited gain range, making it suitable for specific applications. Converters [8-9] have voltage gain of $(2+D_H)/(1-D_H)$ in step-up operation and $D_L/(3-D_L)$ in step-down operation. Converter [9] have low voltage stress and reduced input current ripple across the power MOSFETS but exhibits low voltage gain.

In [10], with voltage gains of $3/(1-D_H)$ and $D_L/3$, a switched-capacitor-based interleaved bi-directional converter is proposed for EV applications, aiming for a higher gain. The circuit in [11] offers high voltage gain of $4/(1-D_H)$ and $D_L/4$ with inherent equal current sharing characteristics. However, converters [10-11] require a high duty ratio to achieve maximum gain, which is not suitable for a wide range of gain applications. Converters [12-14] can achieve extreme voltage with lower duty ratios compared to [10-11]. Converter [12] have voltage gains of $(1-0.33D_H)/(1-D_H)^2$ and $1.5D_L^2$ and uses an intermediate storage capacitor to improve voltage gain and employs a resonant network for ZVS operation. In [13], a quasi-Z-source-based switched capacitor network is proposed with voltage gain $2/(1-2D_H)$ and $D_L^2/(1+D_L)$ to achieve a high conversion ratio at lower duty ratios. However, this converter's gain is limited to duty ratio, increasing control complexity. Converter [14] have voltage gain of $2(3+D_H)/(1-D_H)$ and $D_H/2$ and converter [15] exhibits voltage gain of $1/(1-$

$D_H)^2$ and $D_L^2$. Converters [14-15] are highly suitable for most emerging high-gain applications, they require a larger number of components.

The use of more switches can lead to increased switching losses, resulting in decreased efficiency, and increased system size and cost. Therefore, this work aims to overcome the mentioned drawbacks by proposing a high-gain bi-directional dc-dc converter (HGBDC) for battery storage system applications is presented.

## II. OPERATING PRINCIPLES OF THE PROPOSED BI-DIRECTIONAL CONVERTER

The proposed high gain bidirectional dc-dc converter (HGBDC) incorporates two inductors, four capacitors, and five power MOSFETs as shown Fig. 1(a). The circuit arrangement of step-up mode of operation is shown in Fig. 1(b) and step-down mode operation is shown is Fig. 1(c). Two of the MOSFETs are used in step-up mode, while the remaining three are employed in step-down mode. In addition to improved voltage gain, the proposed converter reduces voltage stress on the MOSFETs.

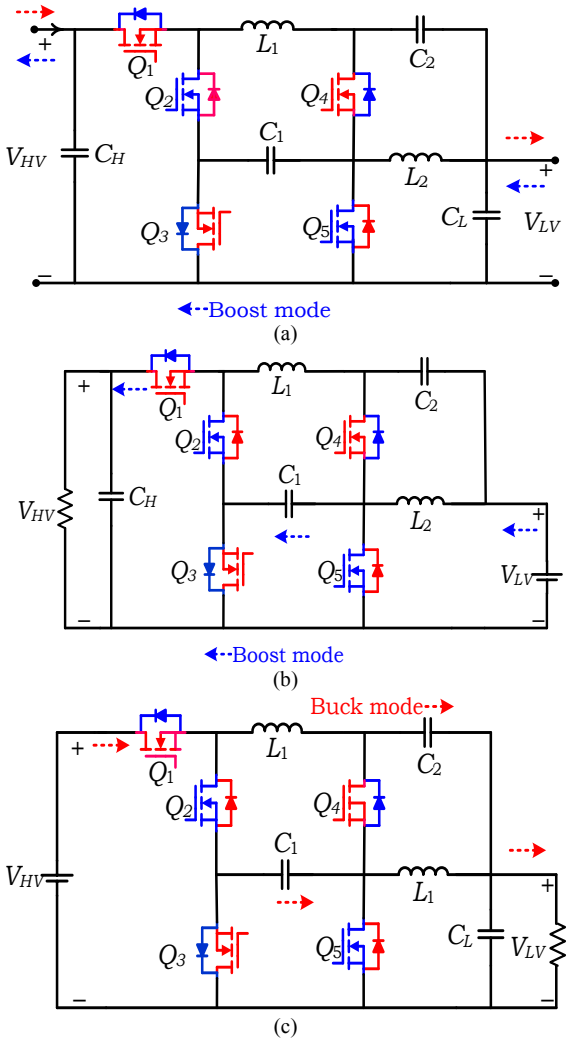


Fig.1 (a) Proposed bidirectional high-voltage gain dc-dc converter (b) step-up mode (c) step-down mode.

### *A. Step-up mode of operation*

The step-up operation of proposed converter is presented under continuous conduction mode (CCM) are shown in Fig. 2(a) and (b) and respective analytical waveforms are shown in Fig. 3(a). Similarly, discontinuous conduction mode (DCM) operation are presented in Fig. 2(a), (b) and (c) and analytical waveforms are shown in Fig. 3(b).

Mode 1 [$t_0$ - $t_1$]: At the time instant $t_0$, $Q_2$ and $Q_5$ are switched ON and $Q_1$, $Q_3$ and $Q_4$ are switched OFF. The equivalent circuit and current-carrying paths of mode 1 are shown in Fig. 2(a). Inductor $L_2$ energies from the low voltage source ($V_{LV}$) via path $V_{LV}$-$L_2$-$Q_5$. Inductor $L_1$ is energized from $C_1$ and $C_2$ via path $V_{L2}$-$V_{C2}$-$V_{L1}$-$Q_2$-$V_{C1}$. Thus voltages across the inductors derived as,

$$V_{L2} = V_{LV} \quad (1)$$

$$V_{L1} = V_{LV} + V_{C1} + V_{C2} \quad (2)$$

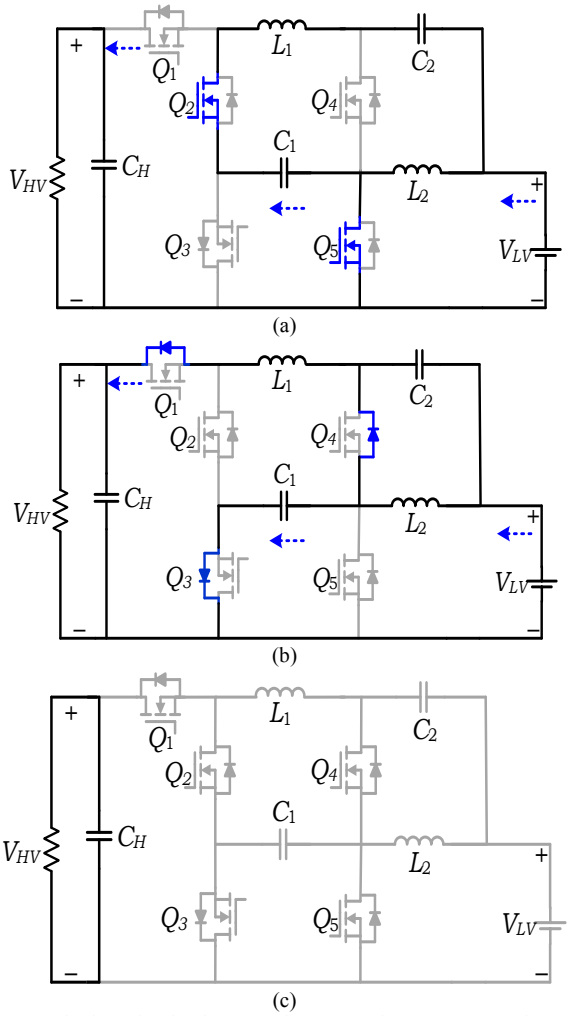


Fig. 2 Equivalent circuit of proposed converter in step-up operation (a) CCM and DCM (b) CCM and DCM (c) DCM.

Mode 2 [$t_1$ - $t_2$]: At time instant $t_1$, anti-parallel diodes of $Q_1$, $Q_3$, and $Q_4$ are turned ON, and where switches $Q_2$ and $Q_5$ are turned OFF. The equivalent circuit and current-carrying paths of mode 2 are shown in the Fig. 2(b). The stored energy in the inductor $L_2$ de-energizes in the path via $V_{LV}$-$V_{L2}$-$V_{C1}$-$Q_3$ and $V_{L2}$-$Q_4$-$V_{C2}$. Inductor $L_1$ de-energies via path $V_{L1}$-$Q_1$-$V_{HV}$-$V_{C1}$. The voltages across the inductors are

$$V_{L2} = -(V_{C1} - V_{LV}) = -V_{C2} \quad (3)$$

$$V_{L1} = -(V_{HV} - V_{C1}) \quad (4)$$

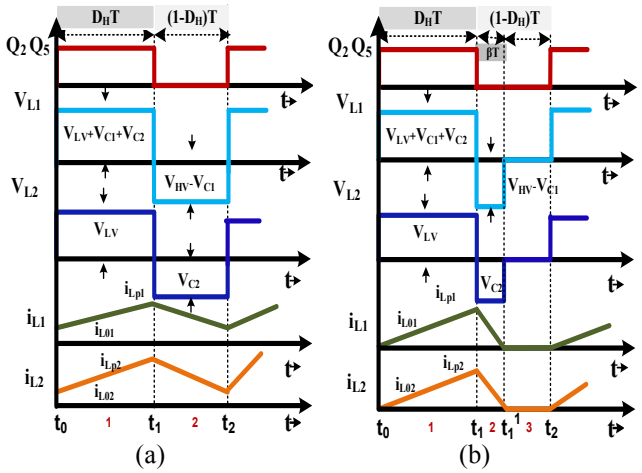


Fig. 3 Analytical waveforms of proposed converter in step-up operation (a) CCM (b) DCM

*B. Step-down mode of operation*

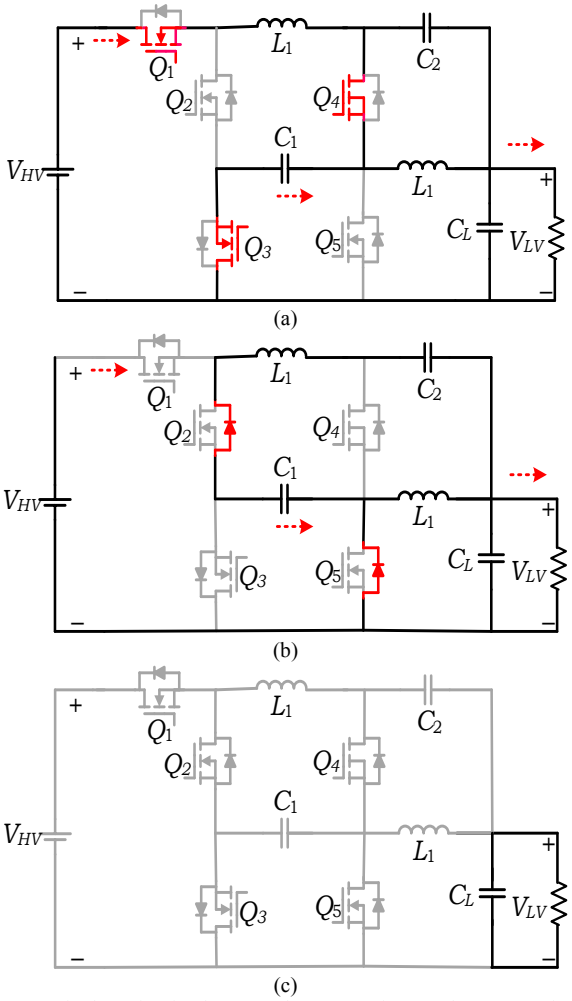


Fig. 2 Equivalent circuit of proposed converter in step-down operation (a) CCM and DCM (b) CCM and DCM (c) DCM.

The step-down operation of proposed converter is presented under continuous conduction mode (CCM) are presented in Fig. 4(a) and (b) and analytical waveforms are presented in Fig. 5(a). Similarly, operation of proposed converter is presented under discontinuous conduction mode (DCM) are presented in Fig. 4(a), (b) and (c) and analytical waveforms are presented in Fig. 5(b).

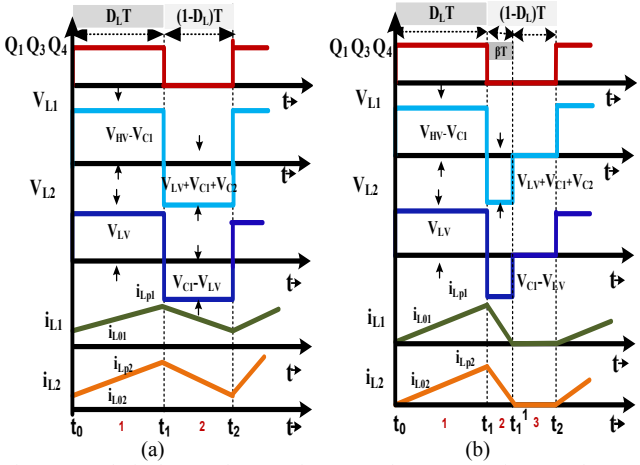


Fig. 5 Analytical waveforms of proposed converter in step-down operation (a) CCM (b) DCM

Mode 1 [$t_0$ - $t_1$]: At time instant $t_0$, the switches $Q_1$, $Q_3$ and $Q_4$ are switched ON, and $Q_2$ and $Q_5$ are turned OFF. The operation in mode 1 of the converter is presented through the equivalent circuit. Inductor $L_1$ energies from high voltage ($V_{HV}$) via current-carrying paths $V_{HV}$-$Q_1$-$V_{L1}$-$Q_4$-$V_{C1}$-$Q_3$, as shown in Fig. 4(a). Inductor $L_2$ energies from via current-carrying paths $Q_3$-$V_{C1}$-$V_{L2}$-$V_{LV}$ and $V_{L2}$-$Q_4$-$V_{C2}$. The voltages across the inductors expressed from the circuit are given below

$$V_{L2} = V_{C1} - V_{LV} = V_{C2} \tag{5}$$

$$V_{L1} = V_{HV} - V_{C1} \tag{6}$$

Mode 2 [$t_1$ - $t_2$]: At time instant $t_1$, anti-parallel diodes of $Q_2$ and $Q_5$ are switched ON, and $Q_1$, $Q_3$ and $Q_4$ are switched OFF as shown in Fig. 4(b). The stored energy in the inductor $L_1$ de-energies via path $V_{L2}$-$V_{C1}$-$D_2$-$V_{L1}$-$V_{C2}$. The inductor $L_2$ starts de-energizes in the path via $V_{LV}$-$D_5$-$V_{L2}$. The voltages across the inductors

$$V_{L2} = -V_{LV} \tag{7}$$

$$V_{L1} = -(V_{LV} + V_{C1} + V_{C2}) \tag{8}$$

## III. STEADY STATE ANALYSIS OF THE PROPOSED BI-DIRECTIONAL CONVERTER

Steady-state gain analysis of proposed converter in step-up mode and step-down mode of operations during CCM and DCM are presented as follows.

*A. Gain analysis of the proposed converter*

*a) Step-up voltage conversion ratio*

From volt-sec balance principle, $L_2$ inductor voltages (1) and (3) are,

$$V_{LV}(D_H) + (-V_{C2})(1-D_H) = 0$$

$$V_{C2} = \frac{V_{LV} D_H}{1-D_H} \tag{9}$$

By substituting (9) in (3)

$$(V_{LV} + V_{C1} + V_{C2}) D_H + (V_{C1} - V_{HV})(1-D_H) = 0$$

$$V_{LV} D_H + V_{C2} D_H + V_{C1} = V_{HV}(1-D_H) \tag{11}$$

$$V_{C1} = \frac{D_H}{1-D_H} \tag{10}$$

From (2) and (4) $L_1$ inductor voltages are,

By substituting (9) and (10) in (11)

$$V_{LV}\left(\frac{1+D_H}{1-D_H}\right)=V_{HV}\left(1-D_H\right)$$

From above voltage gain of the proposed converter in step-up mode of operation is

$$Gain_{step-up}=\frac{V_{HV}}{V_{LV}}=\frac{1+D_H}{\left(1-D_H\right)^2} \quad (12)$$

The equivalent circuit in Fig. 2(c) and analytical waveform in Fig 3(b) are shown under DCM operation. The voltage conversion ratio ($Gain_{step\text{-}up\_DCM}$) in DCM operation under step-up mode is

$$Gain_{step-up\_DCM}=\frac{V_{HV}}{V_{LV}}=\left(\frac{1}{2(D_H-1)}\right)\left(\pm\sqrt{1+\left(\frac{8D_H{}^2}{\tau}\right)}-1\right) \quad (13)$$

From (12) and (13), the time constant ( $\tau_{LB\_step-up}$ ) in step-up operation is derived as,

$$\tau_{LB\_step-up}=\left(\frac{D_H\left(1-D_H\right)^2}{1-D_H}\right) \quad (14)$$

The boundary between CCM and DCM operation of proposed converter in step-up mode is shown Fig. 6(a) and external characteristics are shown in Fig 6(b).

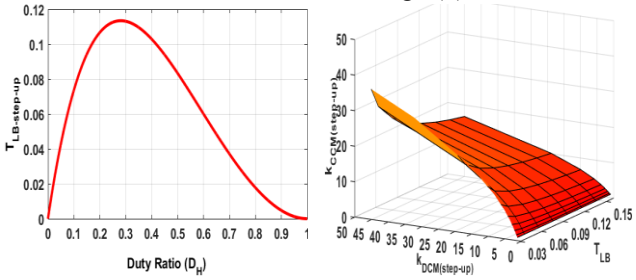


(a) (b)

Fig. 6 (a) boundary condition between CCM and DCM (b) External characteristics of proposed converter in step-up operation

*b) Step-down voltage conversion ratio*

From volt-sec balance principle, $L_2$ inductor voltages (5) and (7) are,

$$V_{C2}\left(D_L\right)+\left(-V_{LV}\right)\left(1-D_L\right)=0$$

$$V_{C2}=\frac{V_{LV}\left(1-D_L\right)}{D_L} \quad (15)$$

By Substituting (15) in (5)

$$V_{C1}=\frac{V_{LV}}{D_L} \quad (16)$$

From (6) and (8) inductor $L_1$ voltages are,

$$\left(V_{HV}-V_{C1}\right)D_L-\left(V_{LV}+V_{C1}+V_{C2}\right)\left(1-D_L\right)=0$$

$$V_{HV}D_L=V_{C1}+V_{C2}\left(1-D_L\right)+V_{LV}\left(1-D_L\right) \quad (17)$$

By substituting (15) and (16) in (17)

$$V_{LV}\left(\frac{2-D_L}{D_L}\right)=V_{HV}D_L$$

From above voltage gain of the proposed converter in step-up mode of operation is

$$Gain_{step-down}=\frac{V_{LV}}{V_{HV}}=\frac{D_L^2}{2-D_L} \quad (18)$$

The equivalent circuit in Fig. 4(c) and analytical waveform in Fig 5(b) are shown under DCM operation. The voltage conversion ratio ($Gain_{step\text{-}down\_DCM}$) in DCM operation under step-down mode is

$$Gain_{step-down\_DCM}=\frac{V_L}{V_H}=\left(\frac{D_L^2(1-D_L)}{\sqrt{2\tau}(2-D_L)}\right) \quad (19)$$

From (18) and (19), the time constant ( $\tau_{LB\_step-down}$ ) in step-down operation is derived as,

$$\tau_{LB\_step-down}=\left(\frac{\left(1-D_L\right)^2}{2}\right) \quad (20)$$

The boundary between CCM and DCM operation of proposed converter in step-down mode is shown Fig. 7(a) and external characteristics are shown in Fig 7(b).

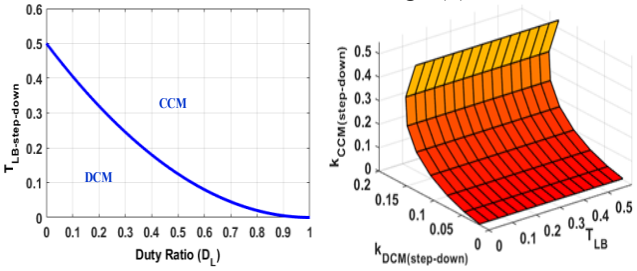


(a) (b)

Fig. 7 (a) boundary condition between CCM and DCM (b) External characteristics of proposed converter in step-down operation

*B. Volatge and current stress analysis*

The voltage stresses of proposed bi-directional converter during step-up and step-down mode of operation are derived in (21) and (22). Similarly, current stresses of proposed converter are during step-up and step-down mode of operation are derived in (23) and (24).

$$\left.\begin{aligned} V_{Q1}&=\left(\frac{\left(1+D_H\right)^2+\left(1-D_H\right)^3}{1+D_H\left(1-D_H\right)^2}\right)V_{HV}\\ V_{Q2}&=V_{HV}\\ V_{Q3}=V_{Q4}=V_{Q5}&=\left(\frac{1-D_H}{1+D_H}\right)V_{HV}\end{aligned}\right\} \quad (21)$$

$$\left.\begin{aligned} V_{Q1}&=\left(\frac{1+D_L}{D_L}\right)V_{LV}\\ V_{Q2}&=V_{LV}\\ V_{Q3}=V_{Q4}=V_{Q5}&=\frac{V_{LV}}{D_L}\end{aligned}\right\} \quad (22)$$

$$\left.\begin{aligned} I_{Q1}&=\left(\frac{1}{\sqrt{1-D_H}\left(1-D_H\right)}\right)I_{LV}\\ I_{Q2}&=\left(\frac{2}{\sqrt{D_H}\left(1-D_H\right)}\right)I_{LV}\\ I_{Q3}&=\left(\frac{2}{\sqrt{1-D_H}\left(1-D_H\right)^2}\right)I_{LV}\\ I_{Q4}&=\left(\frac{1+D_H}{\sqrt{1-D_H}\left(1-D_H\right)^2}\right)I_{LV}\\ I_{Q5}&=\left(\frac{\sqrt{D_H}\left(1+D_H\right)}{\left(1-D_H\right)^2}\right)I_{LV}\end{aligned}\right\} \quad (23)$$

$$\left.\begin{aligned} I_{Q1}&=\left(\frac{D_L\sqrt{D_L}}{\left(2-D_L\right)}\right)I_{HV}\\ I_{Q2}&=\left(\frac{2D_L^2}{\sqrt{1-D_L}\left(2-D_L\right)}\right)I_{HV}\\ I_{Q3}&=\left(\frac{2(1-D_L)}{\sqrt{D_L}\left(2-D_L\right)}\right)I_{HV}\\ I_{Q4}&=\left(\sqrt{D_L}\right)I_{HV}\\ I_{Q5}&=\left(\sqrt{1-D_L}\right)I_{HV}\end{aligned}\right\} \quad (24)$$

*C. Parameter Design*

Based on the current ripples ($\Delta I_L$) and voltage ripples ($\Delta V_C$) of the inductors and capacitors, the sizes of the inductors for both step-up and step-down modes of operation are derived and shown in (25). Similarly, capacitors for both step-up and step-down modes can be derived as shown in (26), respectively. The maximum values from these equations are considered for the final selection of inductors and capacitors.

$$\left.\begin{aligned} L_1 &\geq \frac{2D_H V_{LV}}{\Delta i_{L_1}(1-D_H)f_S} \geq \frac{2(1-D_L)V_{HV}}{(2-D_L)\Delta i_{L_1} f_S} \\ L_2 &\geq \frac{D_H V_{LV}}{\Delta i_{L_2} f_S} \geq \frac{D_L^2(1-D_L)V_{HV}}{\Delta i_{L_2}(2-D_L)f_S} \end{aligned}\right\} \quad (25)$$

$$\left.\begin{aligned} C_H &\geq \frac{D_H I_{LV}}{\Delta V_{HV} f_S}; C_L \geq \frac{(1-D_L)I_{HV}}{\Delta V_{LV} f_S} \\ C_1 &\geq \frac{2I_{LV}}{\Delta V_{C1}(1-D_H)f_S} \geq \frac{2D_L(1-D_L)I_{HV}}{(2-D_L)\Delta V_{C1} f_S} \\ C_2 &\geq \frac{2D_H I_{LV}}{(1-D_H)\Delta V_{C2} f_S} \geq \frac{2D_L^2(1-D_L)I_{HV}}{(2-D_L)\Delta V_{C2} f_S} \end{aligned}\right\} \quad (26)$$

## IV. COMPARATIVE ANALYSIS OF THE PROPOSED BI-DIRECTIONAL CONVERTER

To verify the superiority and performance of the proposed bi-directional DC-DC converter, the most recent reported topologies [6-15] have been considered and compared with the proposed converter across various critical aspects. A detailed comparative analysis is summarized in Table I and voltage gain vs duty ratio plots under step-up and step-down operations are shown in Fig. 8(a) and (b). From this plots, it is clearly indicates that proposed converter achieves higher voltage gain in low duty ratio compared to existing converters with minimum number of components.

TABLE-I

| Topology | [6], 2018 | [7], 2018 | [8], 2021 | [9], 2019 | [10], 2019 | [11], 2021 | [ 12], 2018 | [13], 2021 | [14], 2019 | [15], 2018 | **Proposed** |
|---|---|---|---|---|---|---|---|---|---|---|---|
| $N_S$ | 5 | 4 | 5 | 5 | 8 | 6 | 7 | 7 | 9 | 6 | 5 |
| $N_L$ | 2 | 1 | 3 | 2 | 3 | 2 | 5 | 2 | 2 | 2 | 2 |
| $N_C$ | 4 | 4 | 5 | 6 | 6 | 5 | 6 | 6 | 5 | 3 | 4 |
| $N_T$ | 11 | 9 | 13 | 13 | 17 | 13 | 18 | 15 | 16 | 11 | 11 |
| % $\eta_{max}$ Step-up, $P_O$ | 91.8%, 1kW | 94.3%, 300W | 96.4%, 1kW | 94.09%, 400W | 95.8%, 700W | 95.6%, 1kW | 97.5%, 200W | 96.5%, 300W | 91.4%, 490W | 89%, 200W | 95.3%, 500W |
| % $\eta_{max}$ Step-down, $P_O$ | 91.8%, 1kW | 94.45%, 300W | 96.67%, 1kW | 94.4%, 400W | 95.9%, 700W | 97.7%, 1W | 95.5%, 200W | 91.3%, 300W | 91.3%, 490W | 90.3%, 200W | 95.6%, 500W |
| Step-Up Gain | $\frac{2}{1-D_H}$ | | $\frac{2+D_H}{1-D_H}$ | | $\frac{3}{1-D_H}$ | $\frac{4}{1-D_H}$ | $\frac{1-0.33D_H}{(1-D_H)^2}$ | $\frac{2}{1-2D_H}$ | $\frac{2(3+D_H)}{1-D_H}$ | $\frac{1}{(1-D_H)^2}$ | $\frac{(1+D_H)}{(1-D_H)^2}$ |
| Step-down Gain | $\frac{D_L}{2}$ | | $\frac{D_L}{3-D_L}$ | | $\frac{D_L}{3}$ | $\frac{D_L}{4}$ | $1.5D_L^2$ | $\frac{D_L^2}{1+D_L}$ | $\frac{D_L}{2}$ | $D_L^2$ | $\frac{D_L^2}{2-D_L}$ |

Note: $N_T$ = Total number of components, $N_S$= Number of switches, $N_L$= Number of inductors, $N_C$= Number of capacitors

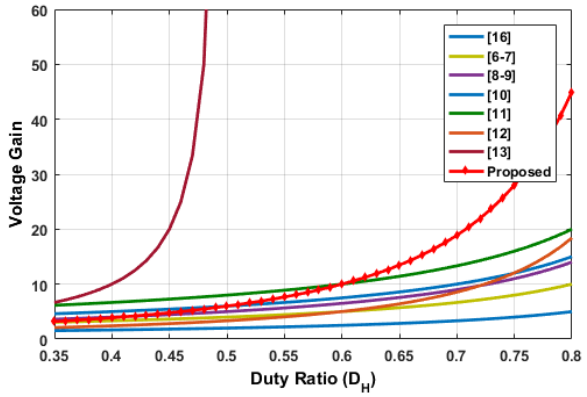


(a)

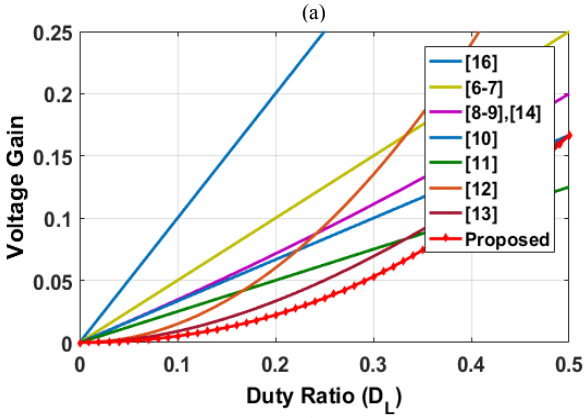


(b)

Fig.8 Comparative analysis gain plot (a) step-up mode (b) step-down mode

## V. SIMULATION RESULTS AND VALIDATION

The simulation results of the proposed converter HGBDC presented in this section. The step-up and step-down mode operations at 500W power and switching frequency of 20 kHz are presented in this paper. During step-up mode of operation, $V_{LV}$=48 V, $V_{HV}$=380 V, $I_{LV}$=11.91 A and $I_{HV}$=1.31 A at duty ratio $D_H$=56% and voltages across the intermediate capacitors $C_1$ and $C_2$ are shown in Fig. 9(a). The voltage and current waveforms of inductors $L_1$ and $L_2$ are presented in Fig. 9(b). Similarly, in step-down mode of operation $V_{HV}$=380 V, $V_{LV}$=48 V, $I_{HV}$=10.4 A and $I_{LV}$=1.8 A at duty ratio $D_L$=44% and voltages across intermediate capacitors $C_1$ and $C_2$ are shown in Fig. 10(a). The voltage and current waveforms of inductors $L_1$ and $L_2$ are presented in Fig. 10(b).

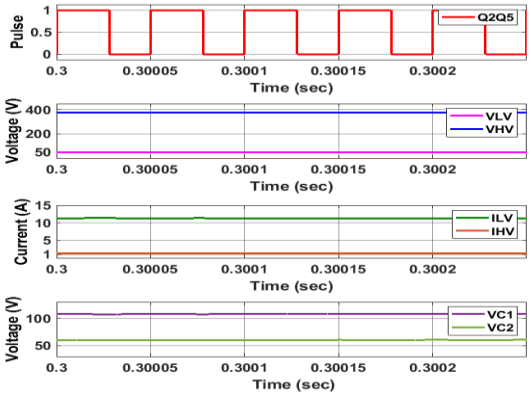


Fig. 9(a) simulation results in step-up operation (i) gate signal (ii) input and output voltages ($V_{LV}$ and $V_{HV}$) (iii) input and output currents ($I_{LV}$ and $I_{HV}$) (iv) capacitor voltages ($V_{C1}$ and $V_{C2}$).

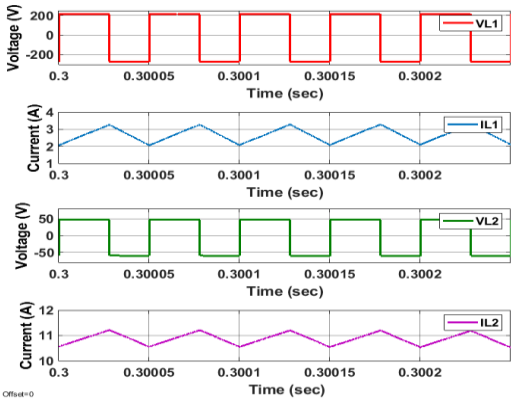


Fig. 9(b) simulation results in step-up operation (i) inductor voltage ($V_{L1}$) (ii) inductor current ($i_{L1}$) (iii) inductor voltage ($V_{L2}$) (iv) inductor current ($i_{L2}$).

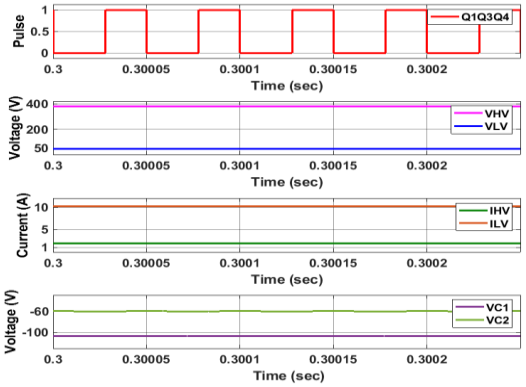


Fig. 10(a) simulation results in step-down operation (i) gate signal (ii) input and output voltages ($V_{HV}$ and $V_{LV}$) (iii) input and output currents ($I_{HV}$ and $I_{LV}$) (iv) capacitor voltages ($V_{C1}$ and $V_{C2}$).

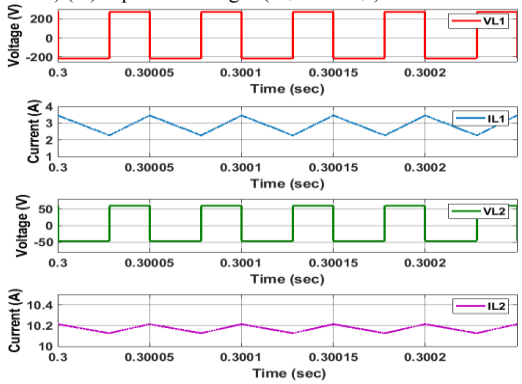


Fig. 10(b) simulation results in step-down operation (i) inductor voltage ($V_{L1}$) (ii) inductor current ($i_{L1}$) (iii) inductor voltage ($V_{L2}$) (iv) inductor current ($i_{L2}$).

## VI. CONCLUSION

In this paper, a high-gain bi-directional DC-DC converter is proposed. The proposed converter is designed to achieve maximum voltage gain with fewer components, thereby reducing the number of switching stags of converters. A 500 W simulation results of the proposed converter presented along with comparative analysis with recent converters to show the superiority. The comparative analysis confirm that the proposed bi-directional DC-DC converter offers high gain at low component count. Additionally, the approach reduces the use of switching converters at each conversion stage, leading to decreased losses, cost, and size. These advantages make the proposed converter most reliable for V2G and G2V applications.

## REFERENCES


[1] Qiu, Dawei, Zihang Dong, Yi Wang, Ning Zhang, Goran Strbac, and Chongqing Kang. "Decarbonising the GB Power System Via Numerous Electric Vehicle Coordination." *IEEE Transactions on Power Systems* (2023).

[2] Blaabjerg, Frede, Yongheng Yang, Ke Ma, and Xiongfei Wang. "Power electronics-the key technology for renewable energy system integration." In *2015 International Conference on Renewable Energy Research and Applications (ICRERA)*, pp. 1618-1626. IEEE, 2015.

[3] Panigrahi, Swetapadma, and Amarnath Thakur. "Current trends in power electronics for wind and solar energy conversion systems." In *2017 International Conference on Power and Embedded Drive Control (ICPEDC)*, pp. 242-247. IEEE, 2017

[4] Ganesan, Swaminathan, Umashankar Subramaniam, Ajit A. Ghodke, Rajvikram Madurai Elavarasan, Kannadasan Raju, and Mahajan Sagar Bhaskar. "Investigation on sizing of voltage source for a battery energy storage system in microgrid with renewable energy sources." *IEEE Access* 8 (2020): 188861-188874.

[5] Forouzesh, Mojtaba, Yam P. Siwakoti, Saman A. Gorji, Frede Blaabjerg, and Brad Lehman. "Step-up DC–DC converters: a comprehensive review of voltage-boosting techniques, topologies, and applications." *IEEE transactions on power electronics* 32, no. 12 (2017): 9143-9178.

[6] Zhang, Yun, Yongping Gao, Jing Li, and Mark Sumner. "Interleaved switched-capacitor bidirectional DC-DC converter with wide voltage-gain range for energy storage systems." *IEEE Transactions on Power Electronics* 33, no. 5 (2017): 3852-3869.

[7] Zhang, Yun, Yongping Gao, Lei Zhou, and Mark Sumner. "A switched-capacitor bidirectional DC–DC converter with wide voltage gain range for electric vehicles with hybrid energy sources." IEEE Transactions on Power Electronics 33, no. 11 (2018): 9459-9469.

[8] Wang, Zhishuang, Ping Wang, Bo Li, Xiaochen Ma, and Peng Wang. "A bidirectional DC–DC converter with high voltage conversion ratio and zero ripple current for battery energy storage system." IEEE Transactions on Power Electronics 36, no. 7 (2020): 8012-8027.

[9] Wang, Zhishuang, Ping Wang, Bo Li, Xiaochen Ma, and Peng Wang. "A bidirectional DC–DC converter with high voltage conversion ratio and zero ripple current for battery energy storage system." *IEEE Transactions on Power Electronics* 36, no. 7 (2020): 8012-8027.

[10] Zhang, Yun, Wei Zhang, Fei Gao, Shenghan Gao, and Daniel J. Rogers. "A switched-capacitor interleaved bidirectional converter with wide voltage-gain range for super capacitors in EVs." *IEEE Transactions on Power Electronics* 35, no. 2 (2019): 1536-1547.

[11] Moradisizkoohi, Hadi, Nour Elsayad, and Osama A. Mohammed. "A voltage-quadrupler interleaved bidirectional DC–DC converter with intrinsic equal current sharing characteristic for electric vehicles." *IEEE Transactions on Industrial Electronics* 68, no. 2 (2020): 1803-1813.

[12] Ashique, Ratil H., and Zainal Salam. "A high-gain, high-efficiency nonisolated bidirectional DC–DC converter with sustained ZVS operation." IEEE Transactions on Industrial Electronics 65, no. 10 (2018): 7829-7840.

[13] Kumar, Avneet, Xiaogang Xiong, Xuewei Pan, Motiur Reza, Abdul R. Beig, and Khaled Al Jaafari. "A wide voltage gain bidirectional DC–DC converter based on quasi Z-source and switched capacitor network." *IEEE Transactions on Circuits and Systems II: Express Briefs* 68, no. 4 (2020): 1353-1357.

[14] Fardahar, Sara Mousavinezhad, and Mehran Sabahi. "New expandable switched-capacitor/switched-inductor high-voltage conversion ratio bidirectional DC–DC converter." IEEE Transactions on Power Electronics 35, no. 3 (2019): 2480-2487.

[15] Pires, Vitor Fernão, Daniel Foito, and Armando Cordeiro. "A DC–DC converter with quadratic gain and bidirectional capability for batteries/supercapacitors." IEEE Transactions on Industry Applications 54, no. 1 (2017): 274-285.

[16] Palanidoss, Sriramalakshmi, and Theja VS Vishnu. "Experimental analysis of conventional buck and boost converter with integrated dual output converter." In 2017 International Conference on Electrical, Electronics, Communication, Computer, and Optimization Techniques (ICEECCOT), pp. 323-329. IEEE, 2017.